

# Computational study of particle in-flight behavior in the HVOF thermal spray process

Mingheng Li, Panagiotis D. Christofides\*

*Department of Chemical and Biomolecular Engineering, University of California, Los Angeles, CA 90095, USA*

Received 22 January 2006; received in revised form 17 May 2006; accepted 31 May 2006

Available online 13 June 2006

## Abstract

A computational framework is developed for the multiphase flow in a high velocity oxygen-fuel (HVOF) thermal spray coating process with steel powders as the feedstock. The numerical model includes continuum-type differential equations that describe the evolution of gas dynamics and multi-dimensional tracking of particle trajectories and temperature histories in the turbulent reacting flow field. The numerical study shows that the particle temperature is strongly affected by the injection position while the particle velocity is less dependent on this parameter. Moreover, both particle velocity and temperature at impact are strongly dependent on particle size, although the spatial variation of these two variables on the substrate is minimal. It is also found that not all the particles are deposited on the substrate perpendicularly (even if the spray angle is  $90^\circ$ ), due to substantial radial fluid velocities near the stagnation point. A statistical distribution of particle velocity, temperature, impinging angle and position on the substrate as well as particle residence time is obtained in this work through independent random tracking of numerous particles by accounting for the distributed nature of particle size in the feedstock and injection position as well as the fluctuations in the turbulent gas flow.

© 2006 Elsevier Ltd. All rights reserved.

*Keywords:* HVOF thermal spray; CFD; Modeling; Particle in-flight behavior; Stochastic particle tracking

## 1. Introduction

The high-velocity oxygen fuel (HVOF) thermal spray is a particulate deposition process in which micro-size particles of metals, alloys or cermets are propelled and heated in a sonic/supersonic combusting gas stream and are deposited on a substrate at high speeds to form a thin layer of lamellar coating. The coatings prepared by HVOF thermal spray process have been widely used in the automotive, aerospace and chemical industries. Representative examples include WC/Co-based wear resistant coatings for drilling tools, YSZ-based thermal barrier coatings for turbine blades, and Ni-based corrosion resistant coatings for chemical reactors. The HVOF thermal spray process is characterized by very high gas and particle velocities

and relatively low gas and particle temperatures, as compared to plasma spray processes. The high particle velocity helps to achieve a high particle flattening ratio at the point of impact on the substrate and to densify the coating. The short residence time in the relatively low temperature gas flame makes the powder particles highly plastic and superheating or vaporization is prevented (Cheng et al., 2003).

It has been shown that the physical and mechanical properties of the HVOF sprayed coatings are directly related to the coating microstructure, which, in turn, depends to a large extent on the physical and chemical states of particles at the point of impact on the substrate (Li et al., 2004a). In order to improve the operation of the HVOF thermal spray process, much experimental work has been done in the last decade to study the effect of operating parameters including gun type, fuel type, feedstock type and size, combustion pressure, fuel/oxygen ratio and spray distance on the particle temperature, velocity, melting ratio, oxidant content and the resulting coating microstructure, porosity, hardness, wear abrasion and corrosion resistance (e.g., de Villiers Lovelock et al., 1998; Gil and Staia, 2002;

\* Corresponding author. Tel.: +1 310 794 1015; fax: +1 310 206 4107.

E-mail addresses: limh@ucla.edu (M. Li), pdc@seas.ucla.edu (P.D. Christofides).

Gourlaouen et al., 2000; Hanson et al., 2002; Hanson and Settles, 2003; Hearley et al., 2000; Khor et al., 2004; Legoux et al., 2002; Lih et al., 2000; Lugscheider et al., 1998; Marple et al., 2001; Planche et al., 2002; Qiao et al., 2003; Suegama et al., 2005; Swank et al., 1994a,b; Wirojanupatump et al., 2001; Zhao et al., 2004). Because of the inherent complexity of the process, a fundamental understanding of the physicochemical phenomena involved in the HVOF thermal spray process generally requires comprehensive numerical models including computational fluid dynamic (CFD) models (e.g., Chang and Moore, 1995; Cheng et al., 2001a,b; Dolatabadi et al., 2003; Gu et al., 2001; Hassan et al., 1998; Kamnis and Gu, 2006; Li and Christofides, 2005; Lopez et al., 1998; Oberkampf and Tallalikal, 1996; Power et al., 1991; Yang and Eidelman, 1996). With the aid of numerical modeling, we might obtain an in-depth understanding of the momentum and heat transfer mechanisms and enhance the performance of thermal spray operation through model-based optimization and control (Chiu and Christofides, 1999; Christofides, 2002).

In a series of previous works, we developed both simplified one-dimensional models (Li and Christofides, 2003; Li et al., 2004a) and a comprehensive CFD model (Li and Christofides, 2005) for the gas dynamics and particle in-flight behavior in the HVOF thermal spray process. These models were integrated into a multi-scale computational framework with a rule-based simulator that predicts the stochastic evolution of coating microstructure (Shi et al., 2004). Based on a comprehensive control-relevant parametric analysis, a feedback control system was developed to control the particle velocity and temperature through the chamber pressure and fuel/oxygen ratio (Li and Christofides, 2004). A modified control system that aims to adjust the particle velocity, temperature and melting degree through direct manipulation of the mass flow rate of fuel and oxygen was also proposed (Li et al., 2004b, 2005). Subsequently, a model-based control scheme that incorporates the estimation of particle properties through the gas phase measurement and particle dynamics was also developed (Li et al., 2004b).

Despite the above computational work and the existing two- or three-dimensional CFD modeling of the gas dynamics in the literature, the particle in-flight behavior is generally based on the centerline of the thermal spray gun and solved by one-dimensional deterministic momentum and heat transfer equations (see, for example, Cheng et al., 2001a; Dolatabadi et al., 2003; Li and Christofides, 2005). However, since the fluid phase is highly turbulent, the particles might be affected by the instantaneous fluctuation in the gas flame. Particles following different trajectories might also experience different heat transfer rates due to the temperature gradient in the gas field. Moreover, as the impinging jet approaches the substrate, the gas velocity in the axial direction decays to zero and the radial velocity becomes substantial near the stagnation point. The objective of this paper is to provide a more realistic description of the particle dynamics through a multi-dimensional random tracking model which explicitly accounts for the distributed nature of particle size in the feedstock and injection position as well as the fluctuations in the turbulent gas flow.

## 2. Model description

### 2.1. Torch design

Fig. 1 shows a schematic diagram of the HVOF torch. The fuel gas (e.g., propylene or hydrogen) reacts with oxygen to produce high temperature combustion gases and a high pressure is maintained in the combustion chamber (the convergent section of the torch). The thermal energy in the gas phase is partially converted to kinetic energy through a convergent–divergent nozzle. With a carefully designed nozzle configuration, the maximum gas velocity can be up to 2000 m/s, with a Mach number around 2 at the exit of the nozzle. The torch body is cooled by air in the convergent section and by water in the divergent section. As the powder particles are injected at the central inlet nozzle using nitrogen as the carrier gas, rapid gas–solid momentum and heat transfer lead to acceleration and heating of the particles. Within several milliseconds, the highly softened powder particles hit the substrate with high velocities and deform as flakes. A lamellar coating structure is formed on the substrate as a result of discrete particle deformation and solidification.

### 2.2. Gas dynamics

The HVOF thermal spray is a multiphase flow process in which the gas dynamics and particle dynamics are coupled with each other. However, because the particle loading in the HVOF thermal spray process is typically less than 4%, the assumption of one-way coupling is usually made (e.g., Li and Christofides, 2005; Yang and Eidelman, 1996). With this assumption the existence of particles has a minimal influence on the gas dynamics, while the particle velocity and temperature can be determined based on the two-phase momentum and heat transfer equations. The governing equations used to describe the thermal spray process are the conservation of mass, momentum, energy, species transport, turbulent kinetic energy and dissipation rate (see Li and Christofides, 2005). Since the direct numerical solution of the instantaneous conservation equations for such a highly turbulent compressible flow is very time consuming, the ensemble-averaged conservation equations might be used so that the small-scale turbulent fluctuations do not need to be directly solved. To convert the Navier–Stokes equations into the ensemble-averaged form, the Boussinesq hypothesis (Hinze, 1975) is usually made to represent the Reynolds stresses (with fluctuation terms) with the mean velocity gradients (without fluctuation terms). However, when the particle dynamics is solved, random fluctuations will be purposely added to the mean fluid field to obtain a more realistic description of the stochastic particle in-flight behavior.

Regarding the combustion chemistry, we note that as the temperature increases above 2000 K, combustion products will dissociate into a number of species with low molecular weight (Cheng et al., 2003, 2001b). Therefore, species with small molecular weight such as CO, OH and H<sub>2</sub> etc. should be included in the combustion products, especially when propylene

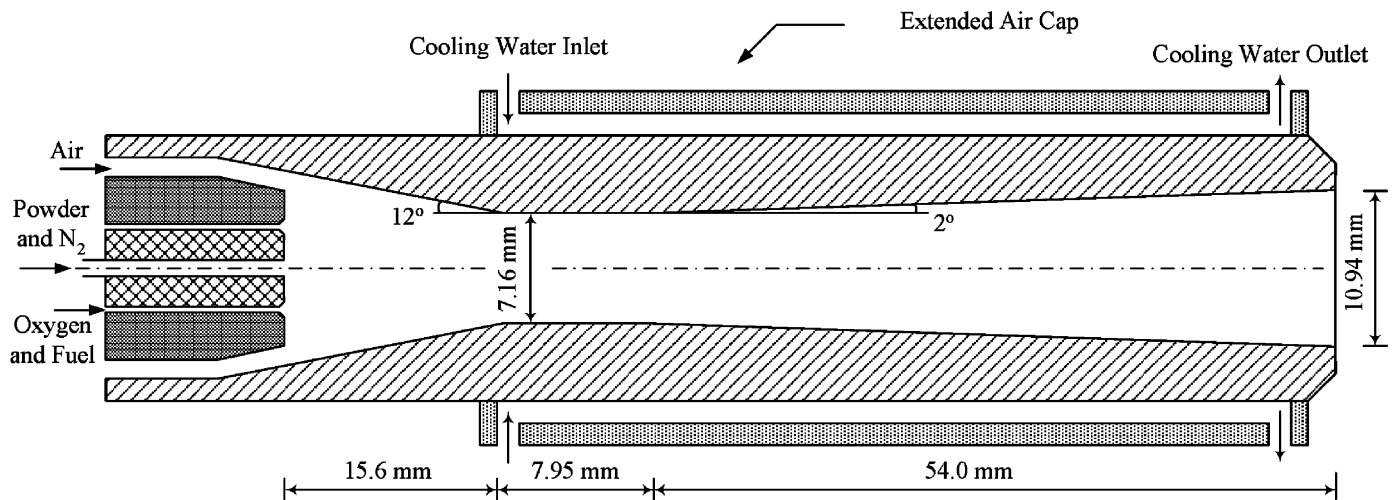
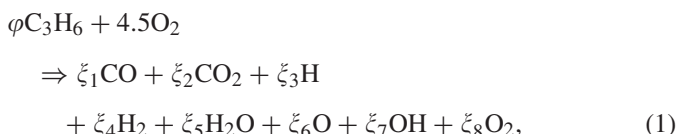


Fig. 1. Schematic diagram of the HVOF thermal spray torch.

is in excess. To accurately model the combustion process with reasonable computational effort, single or multi-step reduced reaction chemistry models might be used (Chang and Moore, 1995; Dolatabadi et al., 2003; Gu et al., 2001; Li and Christofides, 2005; Lopez et al., 1998; Power et al., 1991). In previous studies, different assumptions were made regarding the reaction rate, including: (i) infinitely fast reaction rate (e.g., Cheng et al., 2001a,b; Oberkampf and Talpallikar, 1996; Yang and Eidelman, 1996); (ii) finite reaction rate in Arrhenius form (e.g., Gu et al., 2001; Hassan et al., 1998; Lopez et al., 1998); (iii) finite reaction rate limited by turbulent mixing (e.g., Dolatabadi et al., 2003; Kamnis and Gu, 2006; Li and Christofides, 2005; Power et al., 1991). In this work, we use the eddy-dissipation model, which assumes that the reaction rate is limited by the turbulent mixing rate of fuel and oxidant, or the reaction is instantaneous as the reactants are mixed together. In many practical situations like the HVOF thermal spray process, the eddy-dissipation model describes the limiting rate and thus a knowledge of accurate Arrhenius rate data is not needed (Dolatabadi et al., 2003). Based on the fact that the gas residence time in the combustion chamber (convergent section of the nozzle) is much longer than the subsequent sections, it is assumed that most of the reaction occurs in the chamber and the reaction moves forward following an equilibrium chemistry model. It is also assumed that all the oxygen coming from the air might participate in the reaction (see also Gourlaouen et al., 2000; Li and Christofides, 2005; Li et al., 2004a; Power et al., 1991). Assuming that the air is composed of oxygen and nitrogen only, the reaction considered in this paper is of the following form:



where  $\varphi$  is the equivalence ratio, or the actual fuel/oxygen ratio divided by its stoichiometric value.

However, it is worth noting that the fraction of each species in the combustion gas mixture depends on the combustion pressure, which is unknown before the CFD simulation starts. An approach developed in (Li and Christofides, 2005) is used to determine the chamber pressure. Specifically, we use first a one-dimensional model (Li et al., 2004a) to calculate the combustion pressure based on the flow rate of each gas stream at the entrance of the HVOF torch, and then solve the stoichiometric coefficient involved in Eq. (1) using a chemical equilibrium code with the combustion pressure equal to the partial pressure of oxygen and propylene (Gordon and McBride, 1994). In this way, the pressure obtained by the one-dimensional model is similar to the pressure calculated by CFD simulation, and the amount of trial and error can be significantly reduced.

### 2.3. Particle dynamics

As we mentioned above, due to the very low particle loading, the coupling between the gas phase and the particulate phase is one-way. Therefore, the particle dynamics can be solved after the gas thermal and flow fields are determined. In the particle model development, it is reasonable to assume that the particle coagulation is negligible and the powder size distribution does not change during flight. Also, for typical HVOF thermal spray conditions, the major force acting on a particle is the drag force, and other forces, such as the basset history term, gravitational force and forces caused by pressure gradient and added mass etc., can be neglected (Pawlowski, 1995; Power et al., 1991). Finally, it is assumed that the particles are heated with negligible internal resistance and the internal particle temperature gradients can be ignored due to the small Biot number (ratio of heat transfer coefficient on the boundary to the internal heat conductance) of good heat-conducting particles such as the steel powders considered in the present work. As a result, the equations describing the momentum and heat transfer between a single particle and the fluid take

the form:

$$\begin{aligned} m_p \frac{dv_p}{dt} &= \frac{1}{2} C_D \rho_g A_p (v_g - v_p) |v_g - v_p|, \\ \frac{dx_p}{dt} &= v_p, \\ m_p c_{pp} \frac{dT_p}{dt} &= h A'_p (T_g - T_p) + \varepsilon \sigma A'_p (T_g^4 - T_p^4), \end{aligned} \quad (2)$$

where  $m_p$ ,  $v_p$ ,  $T_p$ ,  $d_p$ ,  $x_p$  and  $c_{pp}$  are the mass, velocity, temperature, diameter, position and heat capacity of the particle, respectively.  $A_p$  is the projected area of the particle on the plane perpendicular to the flow direction.  $A'_p$  is the surface area of the particle.  $v_g$ ,  $T_g$  and  $\rho_g$  are the velocity, temperature and density of the gas phase.  $C_D$  is the drag coefficient, which is a function of the local Reynolds number ( $Re$ ) defined by  $Re = d_p |v_g - v_p| \rho_g / \mu_g$ , where  $\mu_g$  is the gas viscosity. The heat transfer coefficient  $h$  is computed by the Ranz–Marshall empirical equation:

$$h = \frac{\lambda_g}{d_p} [2 + 0.6 Re^{1/2} Pr^{1/3}], \quad (3)$$

where the Prandtl number ( $Pr$ ) is calculated by  $Pr = c_{pg} \mu_g / \lambda_g$ .

#### 2.4. Stochastic particle tracking

Because the fluid flow is highly turbulent, the particles might be affected by the instantaneous fluctuation in the fluid phase. However, as we stated above, the ensemble-averaged Navier–Stokes equation provides only the mean fluid velocity. To address this issue, we employ the stochastic tracking approach (Fluent Inc., 2005) to describe the turbulent dispersion of particles. The approach is based on the instantaneous fluid velocity which is calculated as the sum of the mean fluid phase velocity and a random velocity fluctuation term. The fluctuation velocity component in each spatial direction is kept constant over each time interval and is represented by the characteristic lifetime of the eddies and might change in the next time interval. Specifically,

$$\begin{aligned} v_g &= \bar{v} + v', \\ v' &= \zeta \sqrt{v'^2}, \\ t_L &= 0.15k/\varepsilon, \\ \tau_\varepsilon &= -t_L \log r, \end{aligned} \quad (4)$$

where  $v_g$  is the instantaneous fluid velocity used in Eq. (2),  $\bar{v}$  is the mean fluid velocity solved by the ensemble-averaged conservation equations,  $v'$  is the fluctuation in the fluid velocity,  $\zeta$  is a normally distributed random number, and  $\sqrt{v'^2}$  is the local root mean square of the velocity fluctuations. Based on the assumption of isotropy,  $\overline{v'^2}$  in each spatial direction is the same, therefore,  $3\overline{v'^2}/2 = k$ , or  $\overline{v'^2} = 2k/3$ , where  $k$  is the turbulence kinetic energy in the  $k$ – $\varepsilon$  turbulence model. Finally,  $t_L$  is the fluid Lagrangian integral time,  $\tau_\varepsilon$  is the characteristic lifetime of the eddies, and  $r$  is a uniformly distributed random number between 0 and 1.

Each run of the above discrete random walk model will provide a snapshot profile of particle motion in the gas field. A statistical effect of the turbulence on particle dispersion may be obtained by computing the particle trajectories in this manner for a sufficiently large number of tries.

#### 2.5. Particle size distribution

Because the particle size distribution of the powder particles used in the HVOF thermal spray process is typically polydisperse, and particles of different sizes might have different dynamic behavior during flight due to different momentum and thermal inertias, the process model should account for powder size distribution. Various two-parameter particle size distribution functions exist in the literature such as normal, log-normal and Rosin–Rammler. The Rosin–Rammler distribution function is used in this work while other particle size distribution functions can also be applied in a similar way. The Rosin–Rammler distribution function is particularly suited for representing particles generated by grinding, milling and crushing operations, and is represented by the mean particle size ( $\bar{d}_p$ ) and the spread factor ( $n$ ) as follows:

$$M_{d_p} = \exp[-(d_p/\bar{d}_p)^n], \quad (5)$$

where  $M_{d_p}$  is the retained weight fraction (weight fraction of particles with diameter greater than  $d_p$ ). The parameters used in the Rosin–Rammler distribution function might be determined by plotting  $\ln d_p$  vs  $\ln(-\ln M_{d_p})$ . If a straight line is obtained, then  $n$  is the slope and  $\bar{d}_p$  is the inverse of the exponential of the intercept slope ratio.

### 3. Results and discussion

#### 3.1. Analysis of gas dynamics

The model of gas dynamics represented by continuity, momentum balance, energy balance and species transport (see Li and Christofides, 2005 for details) was implemented into Fluent and was solved by the finite volume method with the segregated solver. The computational domain is shown in Fig. 2. Due to the symmetric geometry of the torch, a one-half, two-dimensional grid is used. The flow is radially symmetric at the centerline. The mass flow rate of oxygen, propylene, air and nitrogen are specified at the opening of each delivery tube upon entering the thermal spray torch. The walls of the torch are all assumed to be at a constant temperature of 400 K. In the external flow field, the radial extent of the computational domain is chosen to be 50 mm. The pressure outlet conditions and wall condition are specified to the outer boundaries and the substrate, respectively. These boundary conditions because of the presence of the substrate are different from those used in free jet flow (Li and Christofides, 2005). The governing conservation equations of mass, momentum, energy and species transport together with the ideal gas state equation are solved first using a first-order upwind scheme to get to a convergent solution and then a second-order upwind scheme to capture the

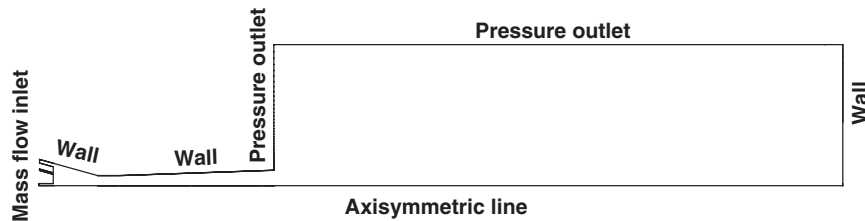


Fig. 2. Computational domain.

Table 1  
Specified gas flow rate in the gas dynamics modeling

Propylene (slm)	Oxygen (slm)	Air (slm)	Nitrogen (slm)	$\dot{m}$ (g/s)	$\phi$
89	139	384	12.5	14.6	1.82

shock diamonds that occur in the external flow field. The gas flow rates of oxygen, propylene, air and carrier gas used in the CFD simulation are shown in Table 1; the values correspond to the recommended flow rates for the processing of metals. It can be readily calculated that the equivalence ratio is 1.82, which is much higher than the one used in the processing of tungsten carbides because the temperature level required for metals is lower than the one for cermets.

The simulated contours of static pressure, density, velocity magnitude, static temperature, Mach number and stream function in both the internal and external fields are shown in Figs. 3–8. In the combustion chamber (convergent section of the air cap), reaction of the oxygen and propylene results in an increase of gas temperature to 2500 K and a high pressure of  $4.6 \times 10^5$  Pa is maintained. As the exhaust gases expand through the convergent–divergent nozzle, the thermal energy in the gas phase is partially converted to kinetic energy. As a result, the pressure and temperature drop and the gas velocity increases along the flow direction. The gas is accelerated to sonic velocity in the flat section, and then to supersonic velocity in the divergent section of the nozzle, reaching a Mach number of 2 at the exit of the nozzle. Because the pressure at the exit of the nozzle is lower than the ambient pressure, the jet is overexpanded and adjusts to the ambient pressure by a series of shock diamonds.

It is worth noting that the gas temperature varies not only in the longitudinal direction, but also in the radial direction. This behavior is significant especially at the entrance of the thermal spray gun, where the cold nitrogen gas is mixed with the high temperature combustion gases. The non-uniform distribution of gas temperature in the internal flow field entails the tracking of particles that enter the thermal spray gun at different radial injection positions, which might follow different trajectories and have different temperature histories. For example, particles enter the thermal spray gun in the centerline might have lower temperature than other particles that are far away from the centerline.

Compared with the gas dynamics in the thermal spray processing of tungsten carbides (see Li and Christofides, 2005), the

gas temperature, velocity and pressure are all lower in the current case. The gas temperature is several hundred degrees lower primarily because the equivalence ratio in this case is much higher than 1, or the oxygen is not adequate to fully oxidize the propylene. This does not imply that not all the propylene participates in the reaction. In fact, because the primary product of the exothermic oxidization reaction is carbon monoxide instead of carbon dioxide when the fuel is in excess, the heat generated by the exothermic oxidization reaction is less. A detailed explanation of this issue can be found in Li et al. (2004a). The pressure in the combustion chamber is also lower in the current case, which might be explained by the following equation:

$$\dot{m}_g = \frac{P_0}{\sqrt{T_0}} A_t \left[ \frac{\gamma \bar{M}_{pr}}{R} \left( \frac{2}{\gamma + 1} \right)^{(\gamma+1)/(\gamma-1)} \right]^{1/2}, \quad (6)$$

where  $\dot{m}_g$  is the total mass flow rate,  $\bar{M}_{pr}$  is the average molecular weight of the reaction product,  $\gamma$  is the specific heat ratio,  $A_t$  is the area of the nozzle throat and  $T_0$  and  $P_0$  are the stagnation temperature and the stagnation pressure, respectively. In the current case, both the total mass flow rate and the stagnation temperature are lower, therefore, the stagnation pressure is also lower. Finally, because the velocity is related to temperature as a function of Mach number (primarily determined by the nozzle configuration), the velocity is lower in the current case because the temperature is lower.

It is also shown that the gas dynamics of the impinging jet in this work has different characteristics from the free jet studied in Li and Christofides (2005). At the stagnation point, the pressure rises due to the conversion of momentum into pressure (see Fig. 3). Also, the axial velocity is converted to radial velocity. According to continuity equation  $(\partial/\partial x)(\rho v_x) + (1/r)(\partial/\partial r)(\rho v_r r) = 0$ , the velocity along the axial direction and radial direction can be estimated by  $v_x = -2bx$  and  $v_r = br$ , respectively, where  $x$  is the distance calculated from the substrate,  $r$  is the distance calculated from the centerline, and  $b$  is a scalar representing the flow strength of the impinging jet (Schlichting and Gersten, 2000). As a result, the gas flows parallel to the substrate (see the stream function shown in Fig. 8) near the substrate. This phenomenon is very important since the particles might move radially due to the drag force in the radial direction. To further demonstrate this behavior, we provide the evolution of the axial velocity and radial velocity of the gas in several different locations in the external flow field, as shown in Figs. 9 and 10. These locations are based on the distance from the exit of the HVOF torch. It is clearly seen that the axial

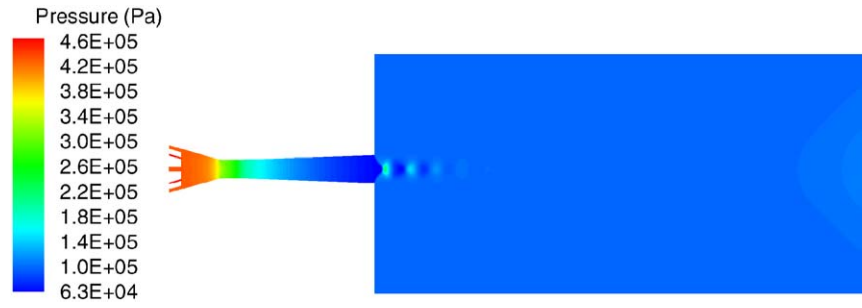


Fig. 3. Contours of pressure.

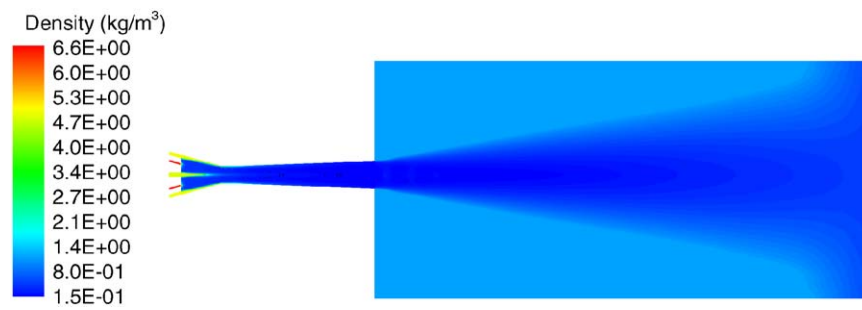


Fig. 4. Contours of gas density.

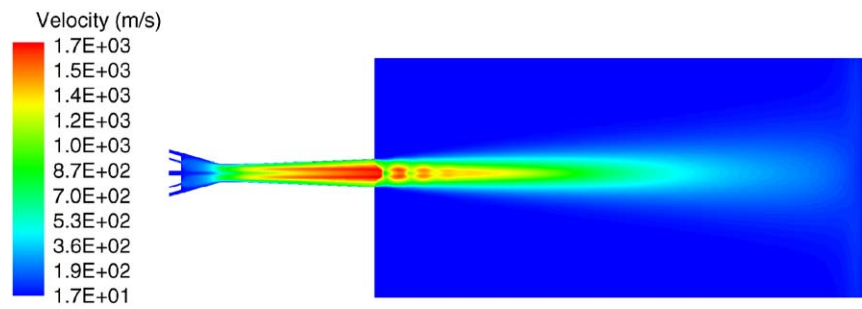


Fig. 5. Contours of gas velocity magnitude.

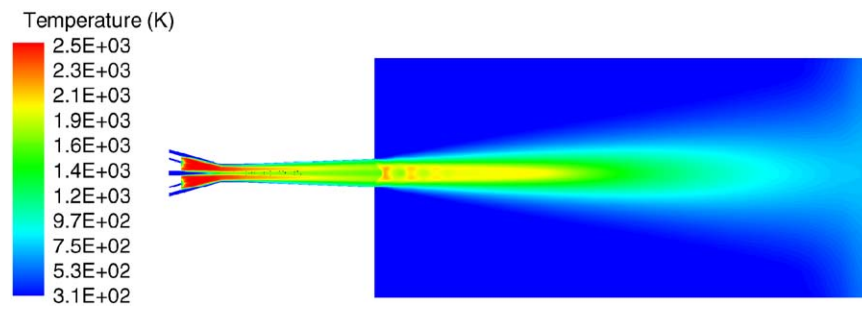


Fig. 6. Contours of gas static temperature.

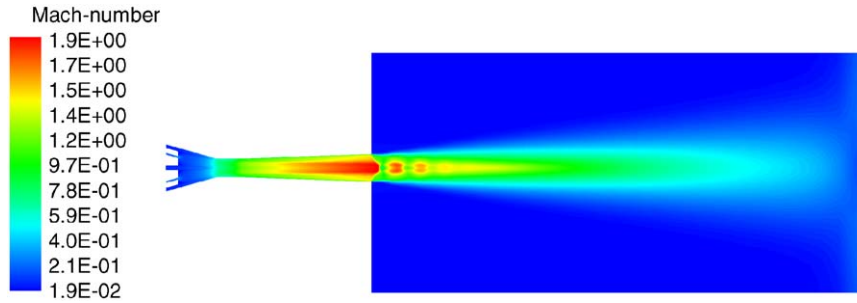


Fig. 7. Contours of gas mach number.

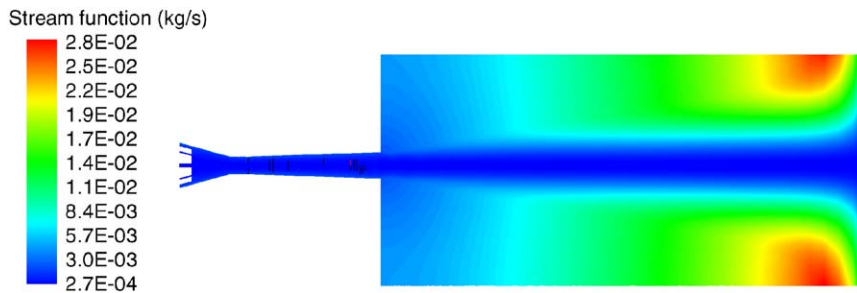


Fig. 8. Contours of gas stream function.

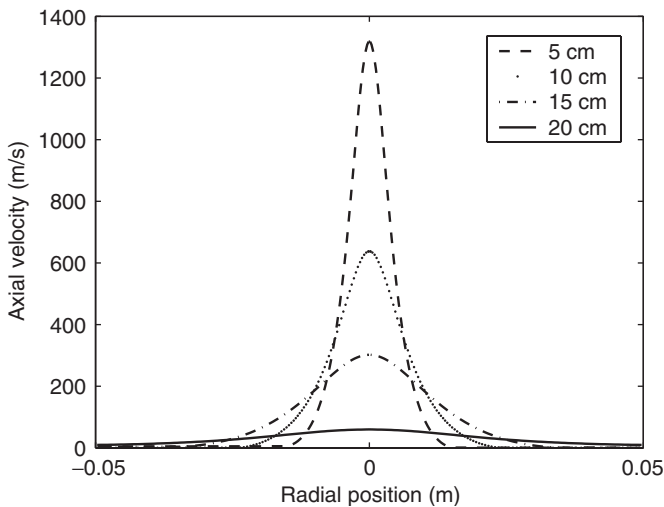


Fig. 9. Axial gas velocity along the radial direction at different axial locations.

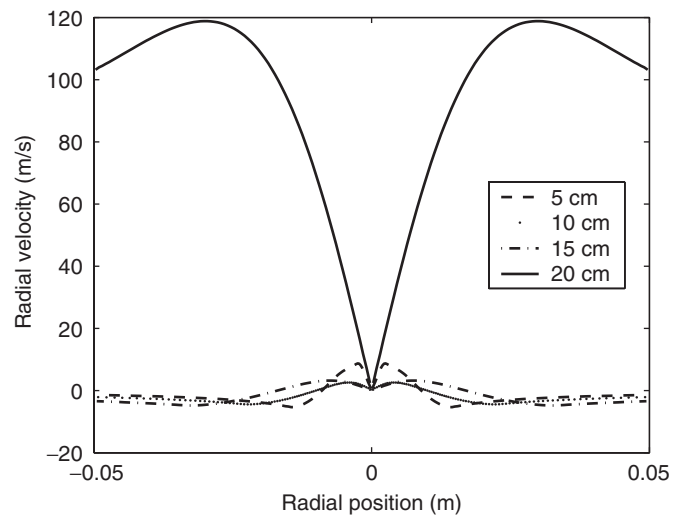


Fig. 10. Radial gas velocity along the radial direction at different axial locations.

velocity in the centerline decays along the axial direction, and the jet propagates outwards in the radial direction. Close to the substrate, the axial velocity profile is close to zero while the radial velocity increases from zero near the stagnation point to more than 100 m/s far away from the centerline.

### 3.2. Influence of injection position on particle velocity and temperature

The microstructure of thermal spray coatings is strongly dependent on particle velocity and temperature at impact on the

substrate. For example, the higher the particle velocity, the denser the coating. Moreover, it is crucial to maintain high particle temperature at the point of impact on the substrate and to prevent particles from being overheated at the same time, especially in the fabrication of nanostructured coatings, because it is exactly the small grain size that leads to the superior qualities of nanostructured coatings (Cheng et al., 2001a). The particle velocity and temperature at impact might be affected by process parameters such as chamber pressure, fuel oxygen ratio, particle size, particle injection velocity and spray distance,

Table 2  
Thermophysical properties of the powder material

Density ( $\text{kg/m}^3$ )	Heat capacity ( $\text{J/kg/K}$ )	Thermal conductivity ( $\text{W/m/K}$ )
8030	502.48	16.27

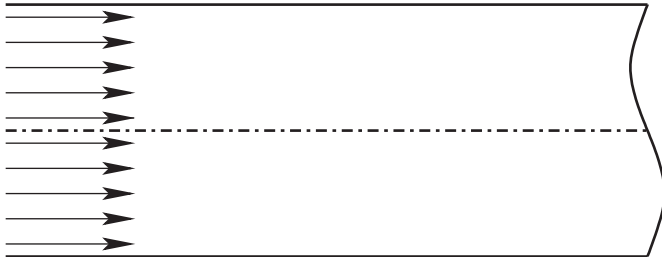


Fig. 11. Distribution of particle injection location in the carrier nitrogen stream.

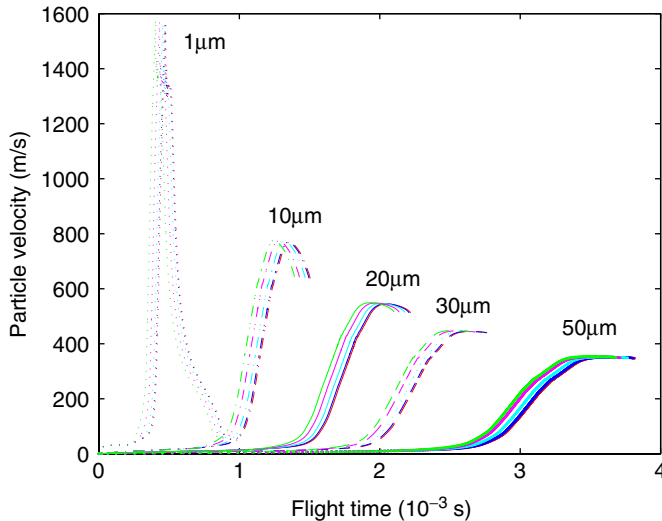


Fig. 12. Evolution of axial velocity of different size particles injected at five different locations as a function of flight time.

which have been studied extensively (e.g., Li and Christofides, 2003, 2004, 2005; Li et al., 2004a, 2005). We also note that the HVOF thermal spray process is characterized by highly turbulent flow and the fluctuations in the flow and thermal fields might lead to variation in the particle velocity and temperature. Moreover, as we mentioned earlier, particles injected at different positions in the carrier nitrogen stream upon entering the convergent section of the torch might follow different trajectories, and therefore, have different dynamic evolution behaviors. The thermophysical properties of the steel powder particles used in the simulation are shown in Table 2.

In this subsection, the effect of injection location (radial location of particles in the carrier nitrogen, see Fig. 11 for details) on these particle properties is first studied and the results are shown in Figs. 12–15. In addition to showing the evolution of particle velocity and temperature with respect to time, we also

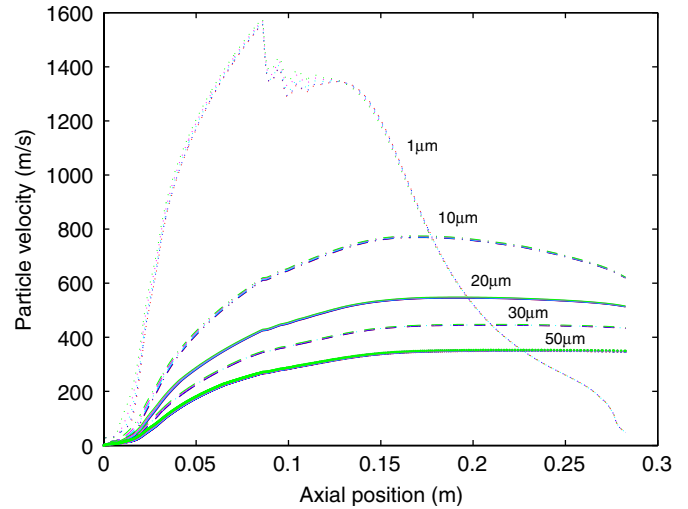


Fig. 13. Profiles of axial velocity of different size particles injected at five different locations as a function of axial position.

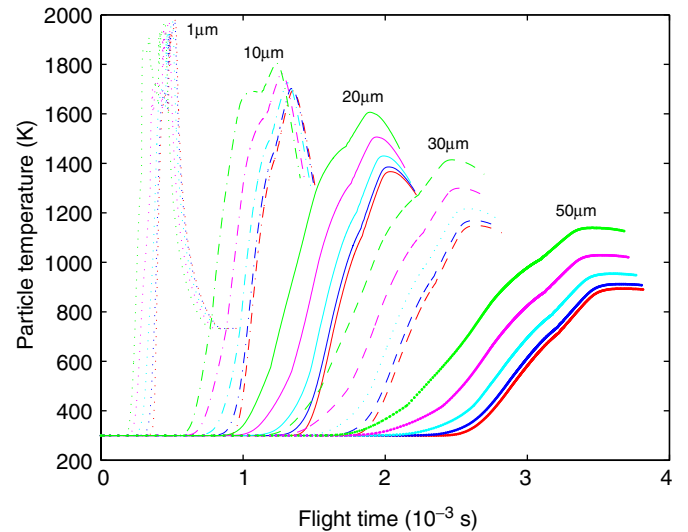


Fig. 14. Evolution of temperature of different size particles injected at five different locations as a function of flight time.

provide the profile of these particle properties along the axial position. These two types of profiles complement each other in demonstrating the particle in-flight behavior in the gas field. It can be seen that for all the particles studied in this work, if they enter the thermal spray gun at different locations with respect to the centerline, they might take different trajectories during flight and might also have different residence times in the gas flame. However, they achieve almost the same velocity at impact when they have the same size. For example, Fig. 12 shows that the evolution of particle velocity is very similar under different injection positions, except for a small time shift in the initial acceleration stage (occurs primarily in the combustion chamber). Fig. 13 also demonstrates that although there is certain difference in the particle velocity in the initial stage, such a difference becomes negligible in a short distance. The particle

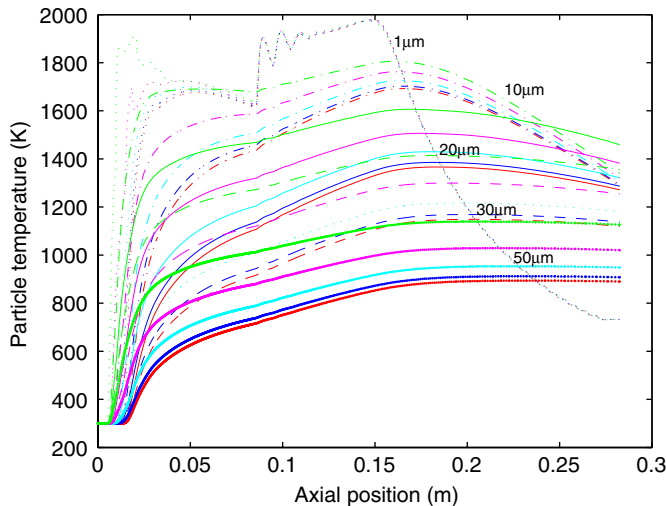


Fig. 15. Profiles of temperature of different size particles injected at five different locations as a function of axial position.

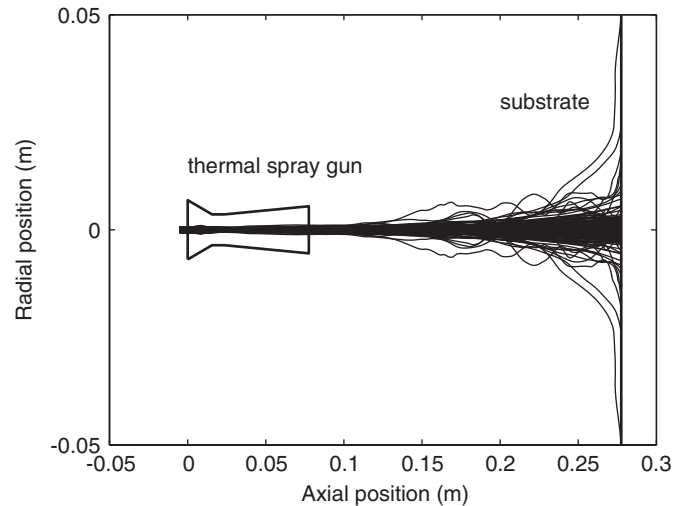


Fig. 16. Trajectories of different size particles injected at different radial positions in the flow field.

temperature at impact, however, is strongly dependent on the injection location if the particle size is larger than  $10\ \mu\text{m}$ , as shown in Figs. 14 and 15. For the same size particles, the difference in the particle impact temperature due to different injection positions might be up to 300 K. This difference occurs in the combustion chamber and reduces along the flow field, but may remain high upon impact on the substrate. The effect of injection position on the particle temperature becomes negligible when the particle size becomes smaller.

To explain these phenomena, we first note that in the gas–solid flow, the driving force for the two-phase momentum transfer (or heat transfer) is proportional to the difference of the velocity (or temperature) in the gas and particulate phase, which implies that the particles eventually achieve the velocity (or temperature) of the gas phase after a long enough time, as long as the gas velocity (or temperature) does not change with respect to time. However, because the residence time of particles in the HVOF field is finite, a characteristic time scale  $\tau = (4\rho_p d_p^2)/(3\mu_g C_D Re)$  can be used to describe the velocity approaching rate ( $\varpi = (d_p^2 \rho_p c_{pp})/(6\lambda_g Nu)$  for particle temperature) (Li and Christofides, 2005; Li et al., 2005). The smaller  $\tau$  is, the faster the particle velocity approaches the gas velocity. Due to the fact that the gas velocity (or temperature) is higher than the one in the particulate phase in the whole internal flow field and part of the external flow field, and becomes lower further downstream, the initial difference in the particle properties in the combustion chamber, if exists, reduces upon impact. In the same sense, if there is a difference in the particle velocity or temperature, it reduces as the particle approaches the substrate, or the difference is compensated for during flight. Finally, the difference in particle properties at impact on the substrate decreases as the particle size decreases.

We note that there is a sharp temperature gradient in the gas phase in the combustion chamber, due to the mixing of the high-temperature oxygen/propylene stream and the low-temperature carrier nitrogen stream. As the particles are injected to the

HVOF torch from different locations in the carrier nitrogen stream, those closer to the high-temperature fuel/oxygen stream will be heated up more quickly. Further, the particle temperature increases as the particle size decreases, which explains why there is a large difference in the initial stage, especially for small particles (see Figs. 14 and 15). A similar phenomenon occurs with respect to the gas velocity. The only difference is that the velocity gradient in the gas phase is not so sharp, and therefore, the resulting difference in the particle temperature is not large either. These initial differences in the particle velocity and temperature are fully compensated for during flight for small size particles (e.g.,  $d_p = 1\ \mu\text{m}$ ) due to small  $\tau$  and  $\varpi$ . However, for large particles, these differences can only be partially compensated for within the finite residence time, which explains that one can still observe the difference in the impact particle temperature (due to large initial difference) but not in the impact particle velocity (due to small initial difference).

In addition, while it is concluded in Li and Christofides (2004) that for particles larger than a certain value, the longer the particle resides in the hot gas stream (due to lower injection velocity), the higher the particle temperature, this conclusion does not apply to the effect of particle injection location on particle temperature. Instead, for large particles ( $d_p \geq 10\ \mu\text{m}$ ), higher particle temperature at impact might correspond to shorter residence time, when the injection position is closer to the fuel/oxygen inlet and the gas velocity is relatively higher.

### 3.3. Influence of turbulent fluctuation in the gas field

Fig. 16 shows a typical snapshot profile of the particle trajectories in the flow field which accounts for the random fluctuation due to turbulence. 100 particles are fed to the HVOF system from 5 uniformly distributed radial locations in the carrier nitrogen stream and 20 uniformly distributed sizes between 1 and  $20\ \mu\text{m}$ . Small particles are used here because they are more sensitive to the fluctuation in the flow field and the effect of

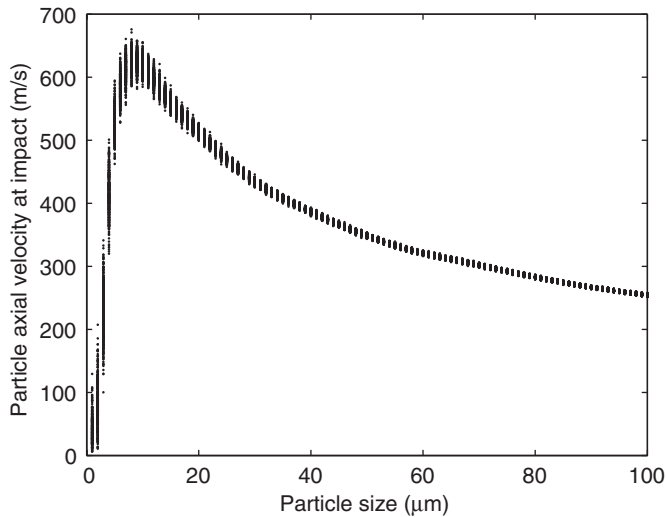


Fig. 17. Axial particle velocity as a function of particle size.

turbulent fluctuation in the gas field can be easily demonstrated. It is seen that although most particles are highly concentrated in the centerline inside of the HVOF torch, the particles tend to expand towards the radial direction when they approach the substrate, due to the increasing radial velocity in the gas phase (refer to Figs. 8 and 10). Small particles (e.g.,  $d_p = 1 \mu\text{m}$ ) are significantly influenced by the gas flow pattern close to the substrate. They are also sensitive to the fluctuation in the gas phase and have more random trajectories. Some of them might even follow the gas stream and will not be deposited on the substrate. Note that submicrometer particles might be deposited on the substrate by thermophoretic force, however, this force is not as strong as the turbulent dispersion. For this reason, particles used in the HVOF thermal spray coating process cannot be too small. This is true even for the processing of nanostructured coatings, in which the powders are comprised of micron-sized agglomerates with grain size below 100 nm.

In the next simulation, 500 particles with particle size from 1 to 100  $\mu\text{m}$  are injected from 5 uniformly distributed locations in the carrier nitrogen stream. Twenty stochastic particle trajectory calculations are performed to obtain a statistical description of the particle velocity and temperature at impact. The results are shown in Figs. 17–20. As expected, the axial velocity of particles with size larger than 20  $\mu\text{m}$  at impact is more robust with respect to the fluctuations in the gas flow field and also the variation in the injection location. Particles with sizes smaller than 20  $\mu\text{m}$ , however, have a wide range of velocity and temperature levels upon impact. The larger the particle size, the less the particle velocity varies with respect to the injection location and the stochastic fluctuations, which can readily explained by  $\tau \propto d_p^2$ .

It is shown in Fig. 18 that not all the particles are deposited on the substrate perpendicularly even if the spray angle is 90°. This is a unique behavior of the impinging flow, which is due to the gas flow pattern close to the substrate. Since particles of very small sizes will closely follow the gas stream (refer to Figs. 8, 10 and 16), as a result, they have lower axial veloc-

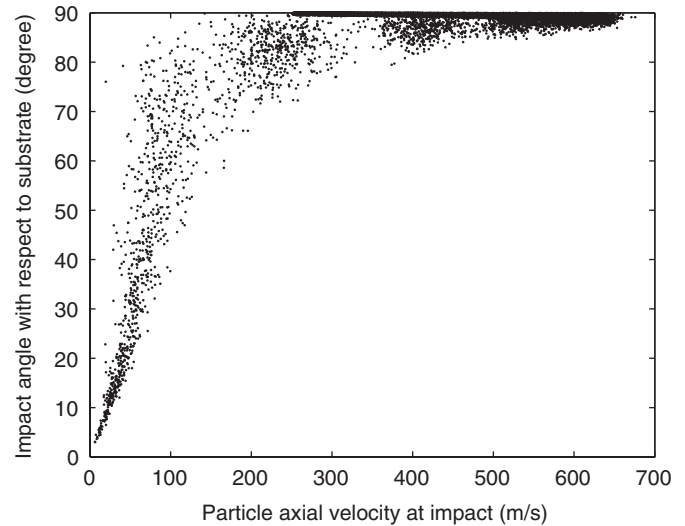


Fig. 18. Particle velocity perpendicular to substrate and impact angle.

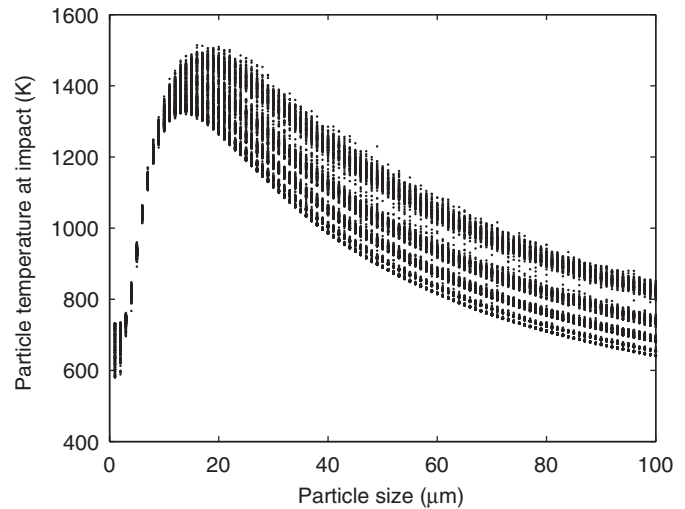


Fig. 19. Particle temperature at impact as a function of particle size.

ity and higher radial velocity than others upon impact as they approach the substrate. That is why it is seen in Fig. 18 that the impinging angle corresponding to axial velocity less than 100 m/s is typically less than 80° or even smaller. When the impact velocity becomes lower than 50 m/s, the impinging angle is less than 30°. The size of the particles should exceed 10  $\mu\text{m}$  in order to be deposited on the substrate fairly straight.

The particle temperature at impact as a function of particle size is shown in Fig. 19. In contrast to particle velocity, the particle temperature is widely spread. This is because large particles ( $d_p \geq 10 \mu\text{m}$ ) are significantly affected by the injection location while small particles ( $d_p < 10 \mu\text{m}$ ) are subject to stochastic trajectories in the gas flame. The variation in the particle temperature caused by these factors is about 100–300 K for all sizes. A mapping of the particle axial velocity and temperature at impact is shown in Fig. 20, which shows that for coarse particles with size larger than 20  $\mu\text{m}$ , the relationship

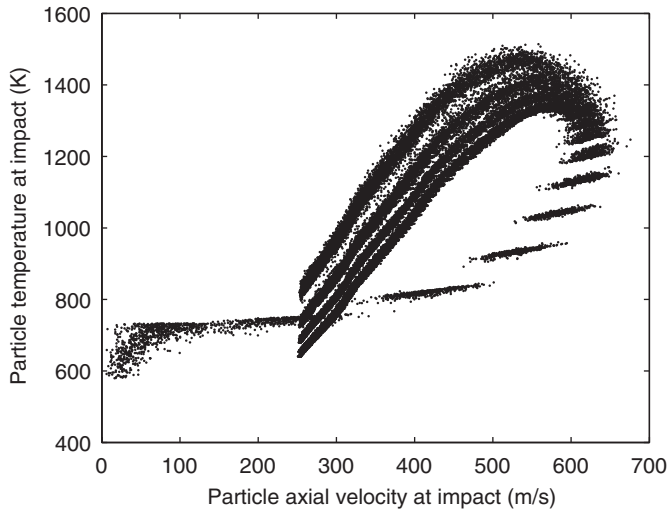


Fig. 20. Mapping of particle velocity and particle temperature.

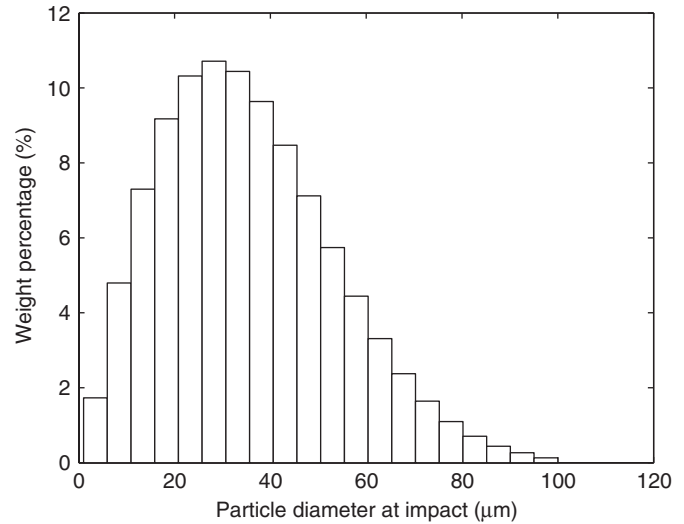


Fig. 21. Distribution of particle size sampled at impact.

of particle velocity and temperature approximately follows a straight line, and both decrease as particle size increases. This mapping supplemented with the particle properties at impact as functions of particle size shown in Figs. 17 and 19 might be used to choose an optimal particle size distribution of the stock material to achieve desired particle temperature and velocity at impact. For example, in order to achieve high particle velocity and temperature at the same time, the particle diameter should be distributed around 20  $\mu\text{m}$ .

### 3.4. Distribution of particle properties at impact

In this subsection, 500 particles of different sizes (1–100  $\mu\text{m}$ ) are fed to the HVOF thermal spray torch and the particle properties are sampled at the substrate. It is assumed that the particles are uniformly distributed across the carrier nitrogen and the particle size follows the Rosin–Rammler distribution. The parameters used in the simulation are  $\bar{d}_p = 40 \mu\text{m}$  and  $n = 2$ . Up to 20 independent stochastic particle tracking calculations are performed to obtain a statistical description of the particle trajectories and temperature histories in the gas flame. Therefore, 50 000 particle trajectories are computed. The simulation shows that less than 0.5% of the particles fully track the gas stream and do not stick on the substrate (note that this model does not account for particle coagulation during flight or particle bouncing off the substrate). As a result, the particle size distribution sampled upon impact is almost the same as the one specified in the injection surface, which follows the Rosin–Rammler distribution. It is also shown that more than 90% of the total volume of the particles are concentrated within 2 mm of the centerline, with an expansion ratio (the ratio of the radius of the impinging circle to the one of the carrier nitrogen) around 3. This is expected because most particles in the size range of 1–20  $\mu\text{m}$  are deposited close to the centerline on the substrate (see Fig. 16). Particles with size larger than 20  $\mu\text{m}$ , due to higher momentum inertia, are even less affected by radial velocity near the substrate (Figs. 21 and 22).

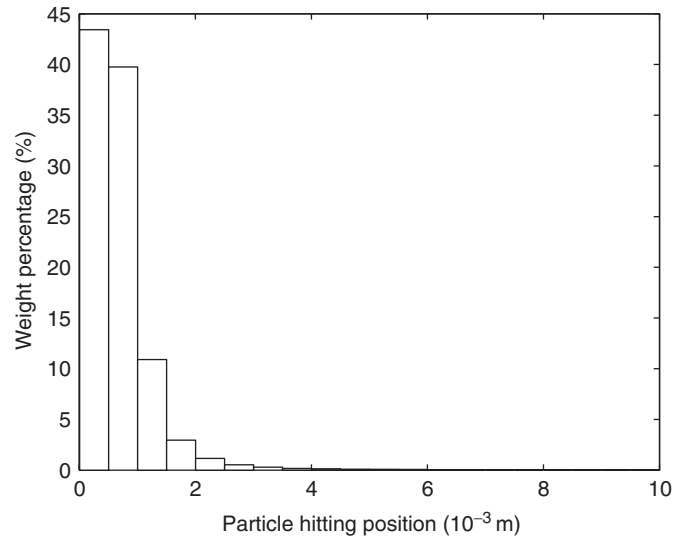


Fig. 22. Distribution of particle hitting position sampled at impact.

The particle residence time in the gas flame approximately follows a normal distribution, as shown in Fig. 23. This is because the residence time is approximately a linear function of the particle diameter. Therefore, the larger the particle size, the longer the particle resides in the HVOF flow field. Most of the particles (based on volume or weight) arrive at the substrate around 2–4 ms, while a small part of the particles have residence time between 0–2 and 4–6 ms.

The distribution of particle velocity and temperature at impact on the substrate are shown in Figs. 24 and 25, respectively. The mean and standard deviation based on the histogram are calculated and it is shown that the particle velocity is  $429 \pm 94 \text{ m/s}$  while the particle temperature is  $1176 \pm 189 \text{ K}$ . The variation in the particle velocity is lower than the one in the temperature because the former is primarily affected by the particle size, while the latter is also influenced by the injection

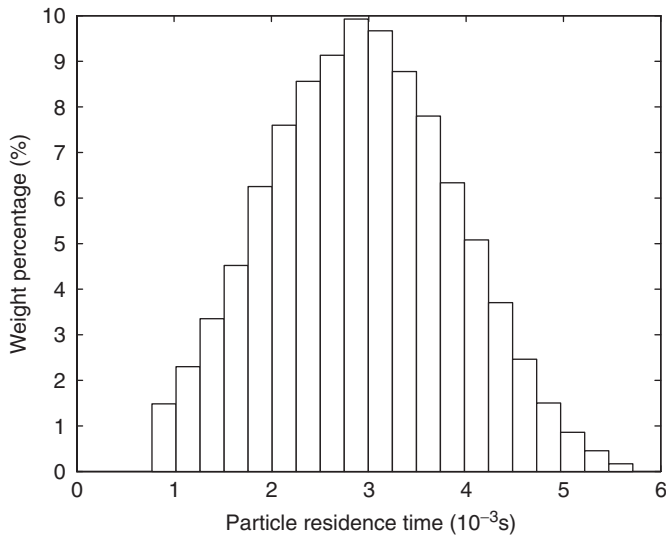


Fig. 23. Distribution of particle residence time sampled at impact.

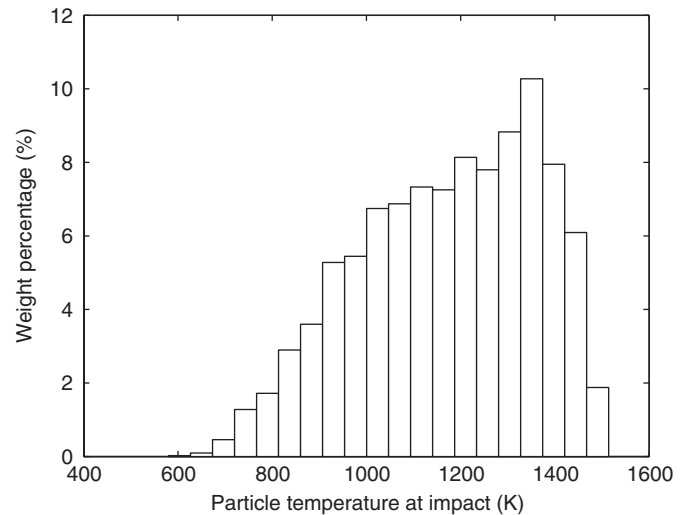


Fig. 25. Distribution of particle temperature sampled at impact.

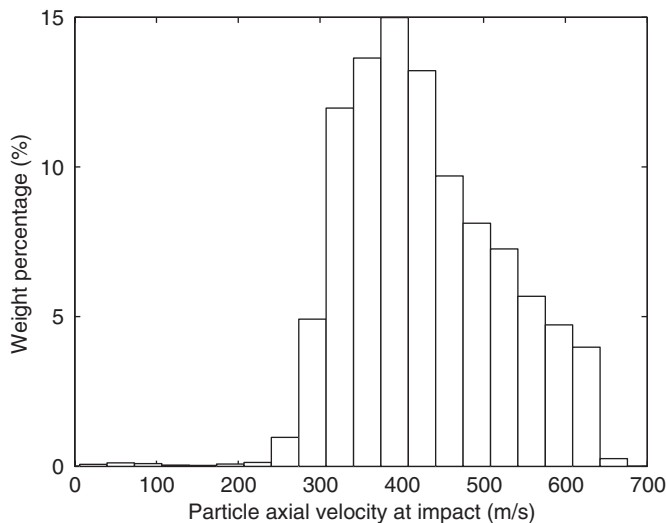


Fig. 24. Distribution of axial particle velocity sampled at impact.

location. The wide distribution of particle velocity and temperature suggests that the optimization and control of the HVOF process should be based on average particle properties.

#### 4. Conclusion

A multi-dimensional stochastic particle tracking model was presented that explicitly accounts for turbulence in the gas phase and distribution of particle size and injection location. The following conclusions were drawn from the parametric model study:

- The particle velocity and temperature are strongly dependent on particle size, although their spatial distribution on the substrate is minimal. The particle size distribution of the feedstock might be optimized to achieve desired particle velocity and temperature levels.

- The particle temperature is strongly affected by the injection position while the particle velocity is more robust with respect to this parameter. Therefore, a possible way to increase the particle temperature is to increase the length of the convergent section of the HVOF gun.
- Not all the particles are deposited on the substrate in a perpendicular way due to high radial gas velocity near the substrate. Very small particles (around 1  $\mu\text{m}$ ) may fully track the gas stream and not adhere to the substrate. Although some of them might be deposited on the substrate, both the impinging velocity and angle are smaller than the ones of large particles.

#### Acknowledgement

Financial support from a 2001 Office of Naval Research Young Investigator Award, program manager Dr. Lawrence Kabacoff, is gratefully acknowledged.

#### References

- Chang, C.H., Moore, R.L., 1995. Numerical simulation of gas and particle flow in a high-velocity oxygen-fuel (HVOF) torch. *Journal of Thermal Spray Technology* 4, 358–366.
- Chiu, T., Christofides, P.D., 1999. Nonlinear control of particulate processes. *A.I.Ch.E. Journal* 45, 1279–1297.
- Cheng, D., Xu, Q., Trapaga, G., Lavernia, E.J., 2001a. The effect of particle size and morphology on the in-flight behavior of particles during high-velocity oxyfuel thermal spraying. *Metallurgical and Materials Transactions B* 32, 525–535.
- Cheng, D., Xu, Q., Trapaga, G., Lavernia, E.J., 2001b. A numerical study of high-velocity oxygen fuel thermal spraying process. part I: gas phase dynamics. *Metallurgical and Materials Transactions A* 32, 1609–1620.
- Cheng, D., Trapaga, G., McKelliget, J.W., Lavernia, E.J., 2003. Mathematical modelling of high velocity oxygen fuel thermal spraying of nanocrystalline materials: an overview. *Modelling and Simulation in Materials Science and Engineering* 11, R1–R31.
- Christofides, P.D., 2002. *Model-Based Control of Particulate Processes*. Particle Technology Series. Kluwer Academic Publishers, Netherlands.

- de Villiers Lovelock, H.L., Richter, P.W., Benson, J.M., Young, P.M., 1998. Parameter study of HP/HVOF deposited WC-Co coatings. *Journal of Thermal Spray Technology* 7, 97–107.
- Dolatabadi, A., Mostaghimi, J., Pershin, V., 2003. Effect of a cylindrical shroud on particle conditions in high velocity oxy-fuel spray process. *Journal of Materials Processing Technology* 137, 214–224.
- Fluent Inc., Lebanon, NH. *Fluent User's Guide*, 2005.
- Gil, L., Staia, M.H., 2002. Influence of HVOF parameters on the corrosion resistance of NiWCrBSi coatings. *Thin Solid Films* 420–421, 446–454.
- Gordon, S., McBride, B.J., 1994. Computer program for calculation of complex chemical equilibrium compositions and applications. NASA Reference Publication 1311, Lewis Research Center, Cleveland, Ohio, USA, 1994.
- Gourlaouen, V., Verna, E., Beaubien, P., 2000. Influence of flame parameters on stainless steel coatings properties. In: *Thermal Spray: Surface Engineering Via Applied Research*, Proceedings of the International Thermal Spray Conference, Montreal, QC, Canada, 2000, pp. 487–493.
- Gu, S., Eastwick, C.N., Simmons, K.A., McCartney, D.G., 2001. Computational fluid dynamic modeling of gas flow characteristics in a high-velocity oxy-fuel thermal spray system. *Journal of Thermal Spray Technology* 10, 461–469.
- Hanson, T.C., Settles, G.S., 2003. Particle temperature and velocity effects on the porosity and oxidation of an HVOF corrosion-control coating. *Journal of Thermal Spray Technology* 12, 403–415.
- Hanson, T.C., Hackett, C.M., Settles, G.S., 2002. Independent control of HVOF particle velocity and temperature. *Journal of Thermal Spray Technology* 11, 75–85.
- Hassan, B., Lopez, A.R., Oberkampf, W.L., 1998. Computational analysis of a three-dimensional high-velocity oxygen fuel (HVOF) thermal spray torch. *Journal of Thermal Spray Technology* 7, 71–77.
- Hearley, J.A., Little, J.A., Sturgeon, A.J., 2000. The effect of spray parameters on the properties of high velocity oxy-fuel NiAl intermetallic coatings. *Surface & Coatings Technology* 123, 210–218.
- Hinze, J.O., 1975. *Turbulence*. McGraw-Hill, USA.
- Kamnis, S., Gu, S., 2006. Numerical modelling of propane combustion in a high velocity oxygen-fuel thermal spray gun. *Chemical Engineering and Processing* 45, 246–253.
- Khor, K.A., Li, H., Cheang, P., 2004. Significance of melt-fraction in HVOF sprayed hydroxyapatite particles splats and coatings. *Biomaterials* 25, 1177–1186.
- Legoux, J.G., Arsenault, B., Leblanc, L., Bouyer, V., Moreau, C., 2002. Evaluation of four high velocity thermal spray guns using WC-10%Co-4%Cr cermets. *Journal of Thermal Spray Technology* 11, 86–94.
- Li, M., Christofides, P.D., 2003. Modeling and analysis of HVOF thermal spray process accounting for powder size distribution. *Chemical Engineering Science* 58, 849–857.
- Li, M., Christofides, P.D., 2004. Feedback control of HVOF thermal spray process accounting for powder size distribution. *Journal of Thermal Spray Technology* 13, 108–120.
- Li, M., Christofides, P.D., 2005. Multi-scale modeling and analysis of HVOF thermal spray process. *Chemical Engineering Science* 60, 3649–3669.
- Li, M., Shi, D., Christofides, P.D., 2004a. Diamond jet hybrid HVOF thermal spray: gas-phase and particle behavior modeling and feedback control design. *Industrial & Engineering Chemistry Research* 43, 3632–3652.
- Li, M., Shi, D., Christofides, P.D., 2004b. Model-based estimation and control of particle velocity and melting in HVOF thermal spray. *Chemical Engineering Science* 59, 5647–5656.
- Li, M., Shi, D., Christofides, P.D., 2005. Modeling and control of HVOF thermal spray processing of WC-Co coatings. *Powder Technology* 156, 177–194.
- Lih, W.C., Yang, S.H., Su, C.Y., Huang, S.C., Hsu, I.C., Leu, M.S., 2000. Effects of process parameters on molten particle speed and surface temperature and the properties of HVOF Cr/CrNiCr coatings. *Surface & Coatings Technology* 133.
- Lopez, A.R., Hassan, B., Oberkampf, W.L., Neiser, R.A., Roemer, T.J., 1998. Computational fluid dynamics analysis of a wire-feed, high-velocity oxygen fuel (HVOF) thermal spray torch. *Journal of Thermal Spray Technology* 7, 374–382.
- Lugscheider, E., Herbst, C., Zhao, L., 1998. Parameter studies on high-velocity oxy-fuel spraying of MCrAlY coatings. *Surface & Coatings Technology* 108–109, 16–23.
- Marple, B.R., Voyer, J., Bisson, J.F., Moreau, C., 2001. Thermal spraying of nanostructured cermet coatings. *Journal of Materials Processing Technology* 117, 418–423.
- Oberkampf, W.L., Talpallikar, M., 1996. Analysis of a high-velocity oxygen-fuel (HVOF) thermal spray torch part 2: computational results. *Journal of Thermal Spray Technology* 5, 62–68.
- Pawłowski, L., 1995. *The Science and Engineering of Thermal Spray Coatings*. Wiley, Chichester, England.
- Planche, M.P., Normand, B., Liao, H., Rannou, G., Coddet, C., 2002. Influence of HVOF spraying parameters on in-flight characteristics of Inconel 718 particles and correlation with the electrochemical behaviour of the coating. *Surface & Coatings Technology* 157, 247–256.
- Power, G.D., Smith, E.B., Barber, T.J., Chiappetta, L.M., 1991. Analysis of a combustion (HVOF) spray deposition gun. Report 91-8, United Technologies Research Center, East Hartford, Connecticut, USA.
- Qiao, Y., Fischer, T.E., Dent, A., 2003. The effects of fuel chemistry and feedstock powder structure on the mechanical and tribological properties of HVOF thermal-sprayed WC-Co coatings with very fine structures. *Surface & Coatings Technology* 172, 24–41.
- Schlichting, H., Gersten, K., 2000. *Boundary Layer Theory*. Springer, Berlin, Germany.
- Shi, D., Li, M., Christofides, P.D., 2004. Diamond jet hybrid HVOF thermal spray: rule-based modeling of coating microstructure. *Industrial & Engineering Chemistry Research* 43, 3653–3665.
- Suegama, P.H., Fugivara, C.S., Benedetti, A.V., Fernández, J., Delgado, J., Guilemany, J.M., 2005. Electrochemical behavior of thermally sprayed stainless steel coatings in 3.4% NaCl solution. *Corrosion Science* 47, 605–620.
- Swank, W.D., Fincke, J.R., Haggard, D.C., Irons, G., 1994a. HVOF gas flow field characteristics. In: *Thermal Spray Industrial Applications*, Proceedings of the Seventh National Thermal Spray Conference, Boston, MA, pp. 313–318.
- Swank, W.D., Fincke, J.R., Haggard, D.C., Irons, G., Bullock, R., 1994b. HVOF particle flow field characteristics. In: *Thermal Spray Industrial Applications*, Proceedings of the Seventh National Thermal Spray Conference, Boston, MA, pp. 319–324.
- Wirojanupatump, S., Shipway, P.H., McCartney, D.G., 2001. The influence of HVOF powder feedstock characteristics on the abrasive wear behaviour of Cr<sub>x</sub>C<sub>y</sub>-NiCr coatings. *Wear* 249, 829–837.
- Yang, X., Eidelman, S., 1996. Numerical analysis of a high-velocity oxygen-fuel thermal spray system. *Journal of Thermal Spray Technology* 5, 175–184.
- Zhao, L., Maurer, M., Fischer, F., Lugscheider, E., 2004. Study of HVOF spraying of WC-CoCr using on-line particle monitoring. *Surface & Coatings Technology* 185, 160–165.